Advances and Potentials of NiO_x Surface Treatments for p-i-n Perovskite Solar Cells

Nidhi Tiwari,[a] Herlina Arianita Dewi[a], Enkhtur Erdenebileg[a], Ram Narayan Chauhan[b] Nripan Mathews [a,c], Subodh Mhaisalkar [a,c] and Annalisa Bruno[a]*

[a] Energy Research Institute @ NTU (ERI@N), Nanyang Technological University, Singapore 637553, Singapore
[b]Department of Physics, NIT Patna, India 800005
[c] School of Materials Science and Engineering, Nanyang Technological University, Singapore 637553, Singapore.

Dr. Nidhi Tiwari, Dr. Herlina Arianita Dewi, Dr. Enkhtur Erdenebileg, Prof. Nripan Mathews, Prof. Subodh Mhaisalkar Dr. Annalisa Bruno.
Energy Research Institute @ NTU (ERI@N), Nanyang Technological University, Singapore 637553, Singapore
Prof. Ram Narayan Chauhan
Department of Physics, NIT Patna, India 800005
Prof. Nripan Mathews, Prof. Subodh Mhaisalkar
School of Materials Science and Engineering, Nanyang Technological University, Singapore 637553, Singapore.
E-mail: Annalisa@ntu.edu.sg

Keywords: perovskite solar cell, p-i-n perovskite solar cells, nickel oxide (NiO_x), surface treatments

Abstract

The performances of perovskite solar cells (PSCs) largely depend on the perovskite compositions and the selection of electron and hole transport layers (ETL and HTL). The p-type NiO_x films have been largely used as HTL in p-i-n PSCs thanks to their high transparency, processing versatility, cost-effectiveness, and easy integration within tandem devices. Several studies have shown that surface modifications on NiO_x films remove the surface defects, increase the NiO_x conductivity, alter the band offset consequently improving the interfaces between NiO_x film and the perovskite active layer. Indeed, besides improving the NiO_x intrinsic properties, the surface treatments also lead, in many cases, to superior perovskite quality driving high photovoltaic performance.

In this review, approaches of surface modifications based on *physical* (UV-ozone, oxygen, argon, and/or helium plasma), *chemical* (interlayer passivation), and *doping* treatments and their impacts on the structural and optoelectronic properties of the NiO_x are examined and discussed. Furthermore, the effects of modified NiO_x films in p-i-n PSCs power conversion efficiency (PCE) are also assessed together with the current challenges and future outlooks.

1. Introduction

Perovskite solar cells (PSCs) represent an economically and environmentally viable option to fulfill the global energy demand. PSCs were firstly developed in 2009 with power conversion efficiency (PCE) of 3.81 %,[1] and in over a decade they reached PCEs as high a 25.5 % for small area devices [2] and over 18% on for mini-modules [3-7]. The record high-performing PSCs are mainly based on n-i-p configuration, while the inverted (p-i-n) PSCs are a bit behind despite their easy fabrication, low-temperature process, cost-effectiveness, and small hysteresis characteristics [8]. To maximize the PCEs and stability of the inverted PSCs and minimodules, the optimization of the electron and hole transport layers (ETL and HTL) and their interfaces with the perovskite layer is critical to promote an efficient charge transfer. An ideal HTL exhibits high hole mobility and conductivity, well-matched energy level with both the perovskite layer and the transparent conducting electrode (*i.e.:* ITO, FTO), large bandgap or low electron affinity (good electron blocking capability), high optical transmittance in the photoactive perovskite range, and no chemical reactivity with the adjacent layers [9]. The most used charge transport materials in inverted PSCs and their corresponding energy levels are summarized in **Figure 1**[8, 10-17].

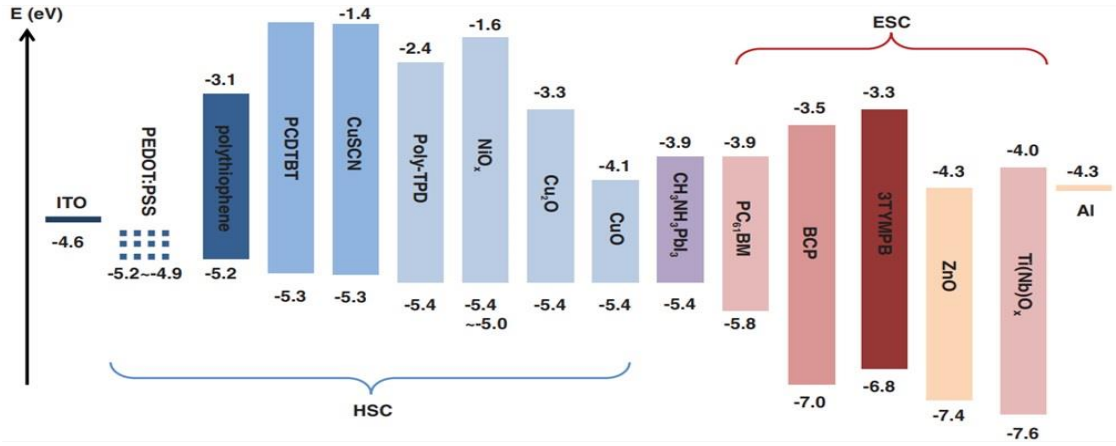

Figure 1 : Energy levels of common materials used as charge transport layers in inverted p.i.n perovskite solar cells. Reprinted from ref 8. Copyright 2016 Wiley-VCH Verlag GmbH & Co. KGaA.

Nickel Oxide (NiO_x) is a low-cost p-type metal oxide showing tunable-optoelectronic properties. NiO_x is considered one of the most promising inorganic hole transport layers for inverted PSCs [18-19] and mini-modules [20-23]. The NiO_x helps to reduce the charge recombination and forms a better ohmic contact with the perovskite layer due to its deep valence band (-5.4 eV) [24-25]. NiO_x has a wide bandgap (> 3.5 eV), high optical transmittance, suitable work function, excellent chemical stability, and a good hole collection efficiency in p-i-n PSCs [26-27]. NiOx can be easily deposited by various methods such as sol-gel[28-29], spray pyrolysis [30-31], sputtering [32-33], evaporation [21, 34], electrochemical [35-36], pulse laser deposition [37], atomic layer deposition [38-39] derived the highest reported PCE of 22.13% for NiOx-based PSCs was obtained with NiO_x films treated with 3,6-difluoro-2,5,7,7,8,8- hexacyanoquinodimethane (F2HCNQ) molecules [40]. The highest PCE for NiOx based minimodules achieved 15.9% for an active area of 10.2 cm^2 where the NiOx was prepared by spin coating. Recently, D. Di Girolamo et al. discussed the NiO_x properties as the most efficient inorganic hole selective layer for halide perovskite photovoltaics in an excellent minireview. The authors reviewed the effect of alkaline and transition metal cations doping, defects, and surface chemistry on the optoelectronic properties of NiO_x and suggest that the performance of the PSCs can be further improved by retarding the segregation of the dopants at the NiO_x interface or avoiding the diffusion inside the perovskite layer. The performance of the PSCs can be further improved by retarding the segregation of the dopants at the NiO_x interface or avoiding the diffusion inside the perovskite layer [41].

Apart from the above salient features, the NiO_x deposition has some limitations. The NiO_x films prepared at room temperature often contain a large number of impurities/surface defects. These may lead to reduced conductivity, hole accumulation at the perovskite interface, high charge carrier recombination, low charge collection, and acceleration of the PSCs degradation [42-50].

Therefore, the film quality needs to be improved to guarantee a wide implementation of NiOx material in applications such as large-area modules, and tandem devices. Few recent works have also shown the potential of atomic layer deposition (ALD) or sputtering processing in producing NiOx films with a reduced density of surface defect and scalable over large areas [32-33, 38-39]. At the moment, the most successful approach to improve the NiO_x conductive, surface defect, and charge separation at the interface with the perovskite are based on surface treatments.

In this review, we discuss the main surface modification strategies based on *physical treatments* (plasma), *chemical treatments* (passivation, interlayer), and *elemental doping* (co-doping) which led to an improved conductivity in NiOx and enhanced charge collection in PSCs, as schematized in **Figure 2**. Moreover, we also discuss challenges and future outlooks on further developments of NiO_x based PSCs

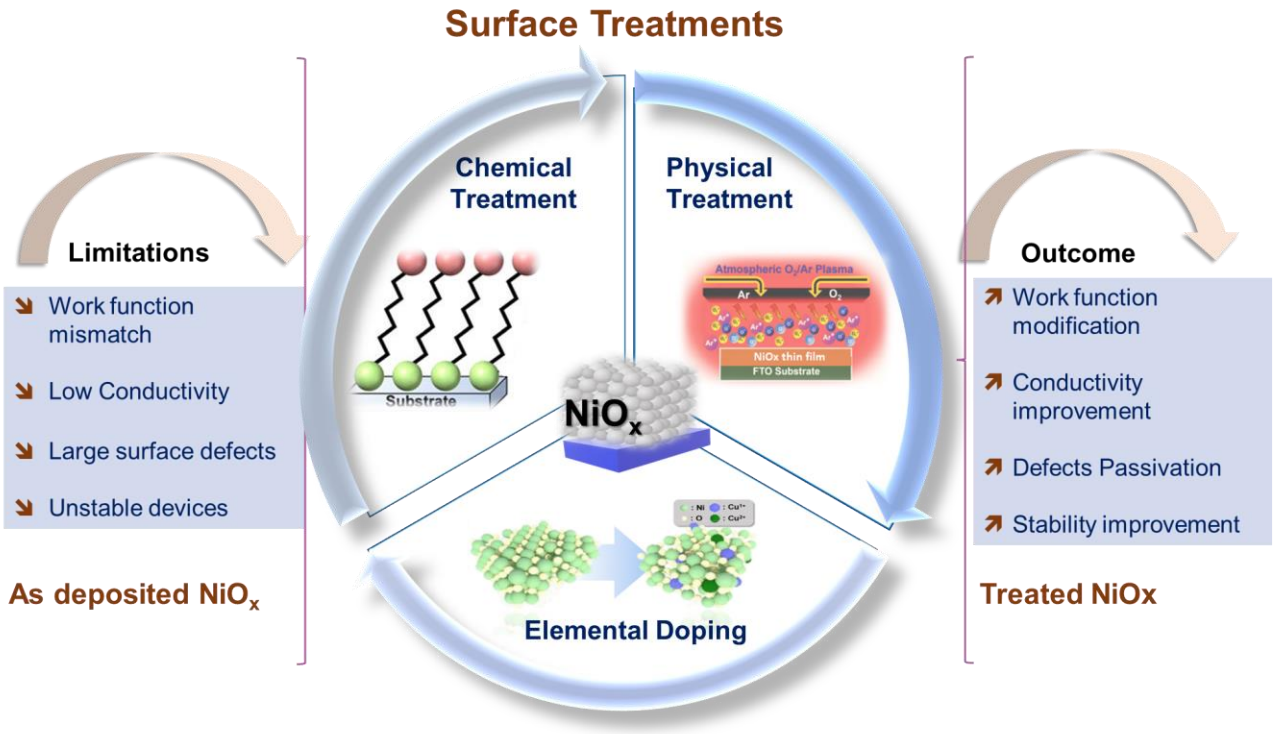

Figure 2: Schematic diagram of the three main types of the surface treatments on NiO_x needed to overcome some intrinsic limitations: chemical treatment, physical treatment, and elemental doping and their outcomes on the film quality.

2. Surface modifications by physical processes

Several works have shown that physical surface treatments increase the NiO_x intrinsic conductivity, improve the band alignment with the perovskite, and increase the electron blocking efficiency [51-53]. Hereafter we will describe the effects of UV-Ozone, argon, nitrogen, and oxygen plasma treatments on the physical and optoelectronic properties of the NiO_x thin films. Recent results based on this strategy are summarized in **Table 1**.

2.1 UV Ozone Plasma Treatment

The UV/ozone treatment provides good film quality with improved work function and electrical conductivity which are desirable properties for the fabrication of high efficiency and stable PSCs. Islam et al. demonstrated that the UV-ozone treatment changes both the surface properties and the compositions (towards oxygen-rich stoichiometry) throughout the whole depth of the film, **Figure 3a** [54]. The oxygen-rich stoichiometry creates nickel vacancies, rather than the oxygen interstitials in NiO_x film, which introduce localized defect states near the valence band. These defects reduce the hoping transport barrier for holes significantly increasing the conductivity of the NiO_x film [54-57]. Moreover, the UV-ozone treatment creates dipolar species of nickel oxyhydroxide (NiOOH) on the NiO_x surface which are responsible for an increase of the work function.

T. Wang et. al. studied the effects of the UV-ozone treatment on the physical, chemical, and optoelectronic properties of the NiO_x films electrochemical processed and annealed at 300 °C for 2 h. The UV-ozone exposure of NiO_x film for 5 min resulted in higher hydrophilicity which facilitates the formation of a very uniform perovskite layer while maintaining a NiO_x good electrical conductivity (2.89×10^{-6} S/cm) and transparency (~85% in the visible region). The UV-ozone exposure modified the work function (4.86 eV) and shift the valence band maximum (5.34

eV) of NiO_x thin film close to the one of the $MAPbI_3$ perovskite (5.47 eV), **Figure 3b**. The PSC with the treated NiO_x (UVO-NiO_x) achieved a PCE of 19.67%, **Figure 3b**. The V_{oc} and J_{sc} increased from 1.01 V to 1.11 V and from 21.69 mA cm^{-2} to 23.41 mA cm^{-2}, respectively as compared to the pristine NiO_x. Long term stability tests, carried out on encapsulated PSCs in an inert environment (H_2O <1 ppm and O_2 <0.1 ppm) and at room temperature, showed that the PSCs with pristine NiO_x and UVO-NiO_x retained respectively ~80% and ~84% of their initial PCEs for over 40 days of storage[19].

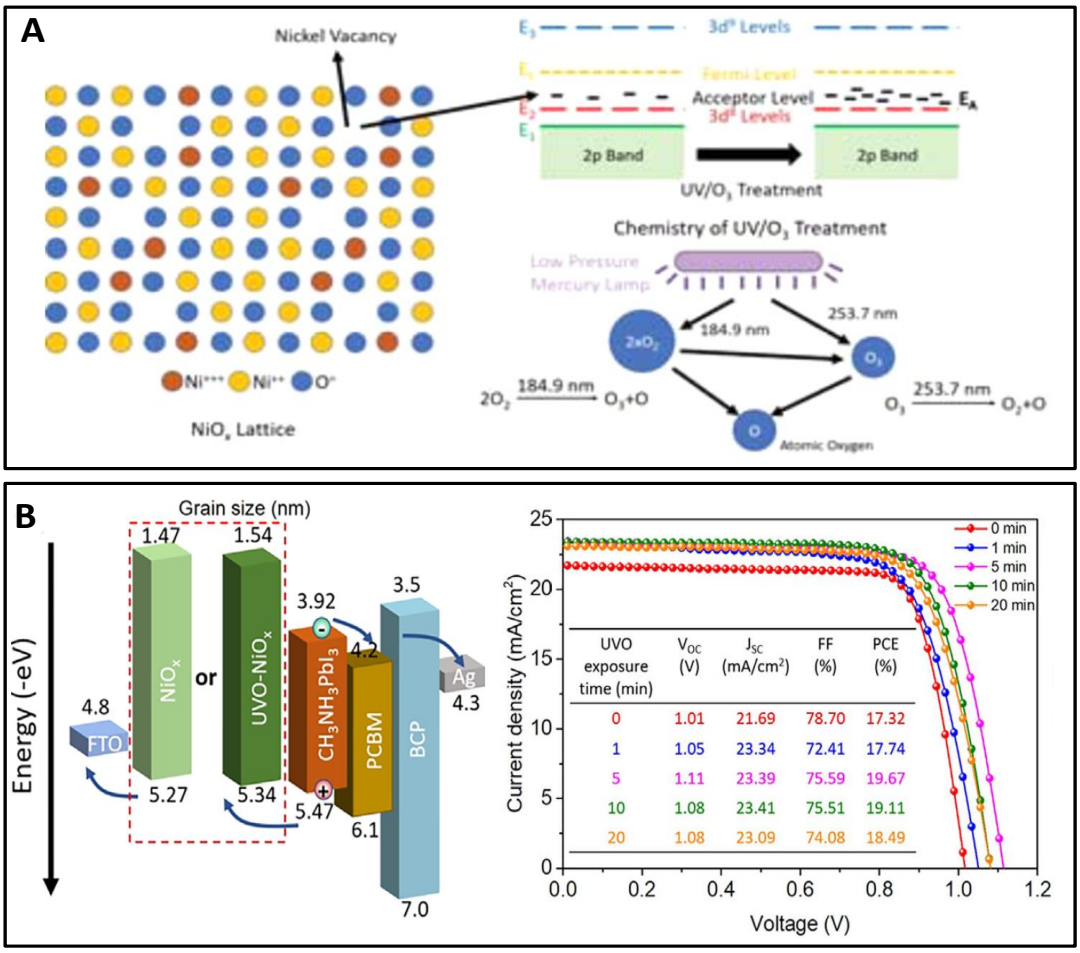

Figure 3. A Illustration of the formation of nickel vacancies in NiO_x under the UV-ozone treatment. Reprinted from ref 54. Copyright 2017 American Chemical Society. **B** Left: Schematic representation of the energy band diagram for the PSC (with a structure of FTO/NiO_x/$MAPbI_3$/PCBM/BCP/Ag). Right J–V curves of optimal PSC devices based on UVO-treated NiO_x HTL with different exposure times. Reprinted from ref 19. Copyright 2019 Wiley-VCH Verlag GmbH & Co. KGaA

2.2 Oxygen, Argon, and/or Helium Plasma Treatment

Oxygen plasma is an effective method to modify the surface chemistry of the NiO_x nanoparticles film as it can remove all traces of the chemisorbed layer [58]. J Zhang et al. explained the formation of NiOOH species on the surface of the solution processed NiO_x nanoparticles under oxygen plasma treatment. The presence of NiOOH species improves the work function (-5.3 eV) of the NiO_x nanoparticle like the case observed during UV-ozone treatment [59-60].

N Pant et al. demonstrated that the oxygen plasma treatment on sputtered NiO_x layer increases the $Ni^{3+/}Ni^{2+}$ ratio, enhances the surface wettability, and improves the morphology of the perovskite layer overlaid on the NiO_x. The superior NiO_x properties result in the suppression of interfacial defects and recombination which boosts PSCs performance as shown in **Figure 4a** [61]. X. Zheng et al. demonstrated that the low-power (10 W) oxygen plasma treatment on the annealed NiO_x film (T=250°C, named as NiO_x-250°C-10 W) allowed the PSCs to reach photovoltaic values of V_{oc} of 1.083 V, FF of 78.5%, and PCE of 18.38%. The performance of the PSCs tends to degrade instead under higher power oxygen plasma. The authors suggest that further chemical passivation of NiO_x suppresses the bulk/interface defects, minimizes the device hysteresis, and efficiently reduces the insulating $Ni(OH)_2$. The chemical passivation of KCl (20 mg ml^{-1}) with 20-30 W O_2-plasma (device named NiO_x-250°C-K 20–30 W) resulted in improved device performance (J_{sc} ~ 23.27 mA cm^{-2}, V_{oc} ~ 1.049 V, FF~78.8% and PCE ~19.16%) with reduced hysteresis, **Figure 4b.** In addition, the PSCs with optimized NiOx layer (NiOx-250 1C-K 20–30 W) maintained 88% of their initial PCEs after 660 min at maximum power point (MPP) tracking under continuous AM1.5

illumination without encapsulation. The shelf lifetime shows that the PSCs maintain also 75% of their initial PCEs after 600 h aging with RH higher than 80% [62].

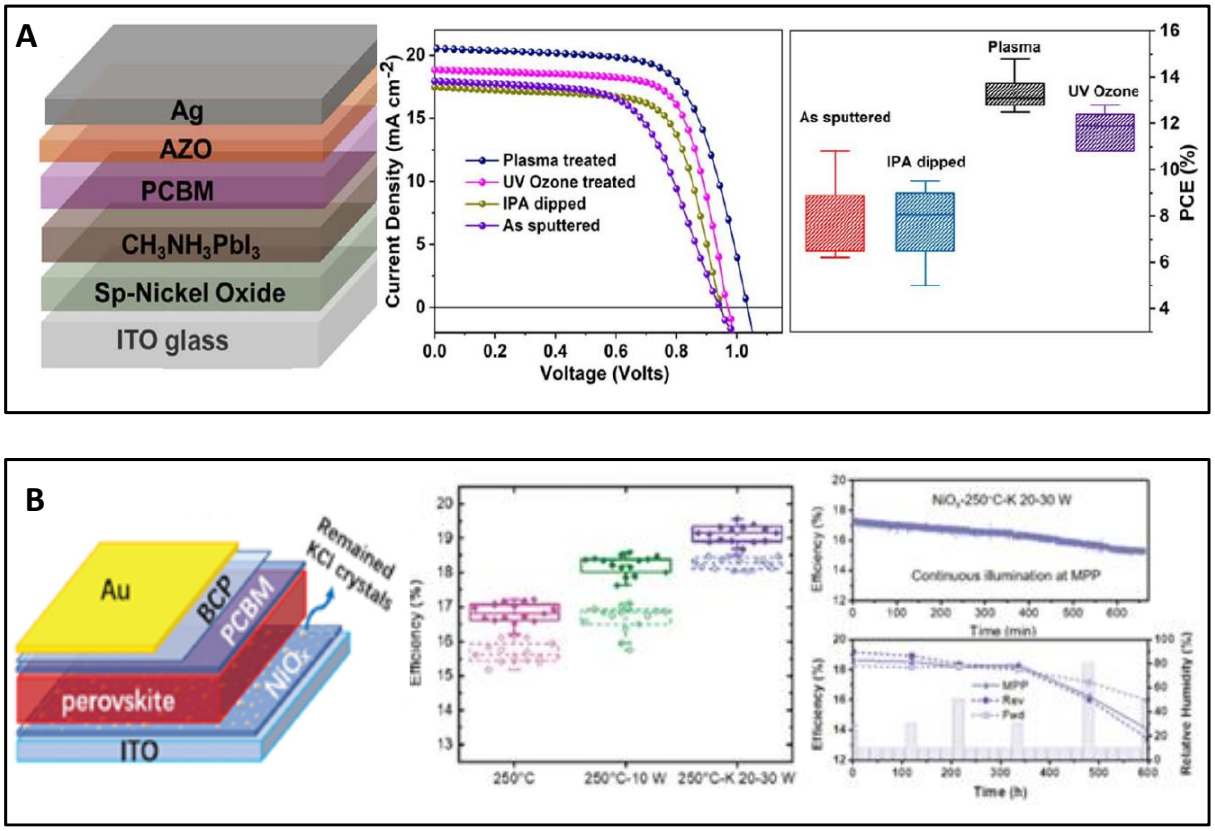

Figure 4: A Left side: Schematic illustration of PSCs architecture. Middle; J-V curves of the best performing PSCs with various treatment conditions; Right side: PCE distribution of the PSCs with different conditions. Reprinted from ref 61. Copyright 2020 The Japan Society of Applied Physics. **B.** Left side: Schematic illustration of PSCs architecture. Middle PCEs statistical distribution of three types of PSCs NiOx-250℃, NiO_x-250℃-10 W, NiO_x-250℃-K 20–30 W for both forward and backwards directions. Right side: The illumination stability (top) and long-term stability (bottom) of the device with optimized NiOx-250℃-K 20–30 W HTL. Reprinted from ref 62. Copyright 2020 The Royal Society of chemistry.

J.-H. Tsai et al. demonstrated that using the atmospheric-pressure dielectric-barrier-discharge-jet (DBDjet) helium plasma treatment the quality of NiO_x films significantly improved, **Figure 5**. The authors used the DBDjet treatment, with a scan rate of 0.2cm/s, on NiO_x film reduced the $Ni(OH)_2$ content and increased O−C=O and C−O contents (hydrophilic functional groups). This treatment led to deeper valance band maxima (VBM) and a more suitable band alignment within the PSCs.

The PSCs with the treated NiO_x exhibited a PCE (~14.88%) as compared to the untreated NiO_x based device where the PCE reached 13.63% (PCE~13.63%) [63].

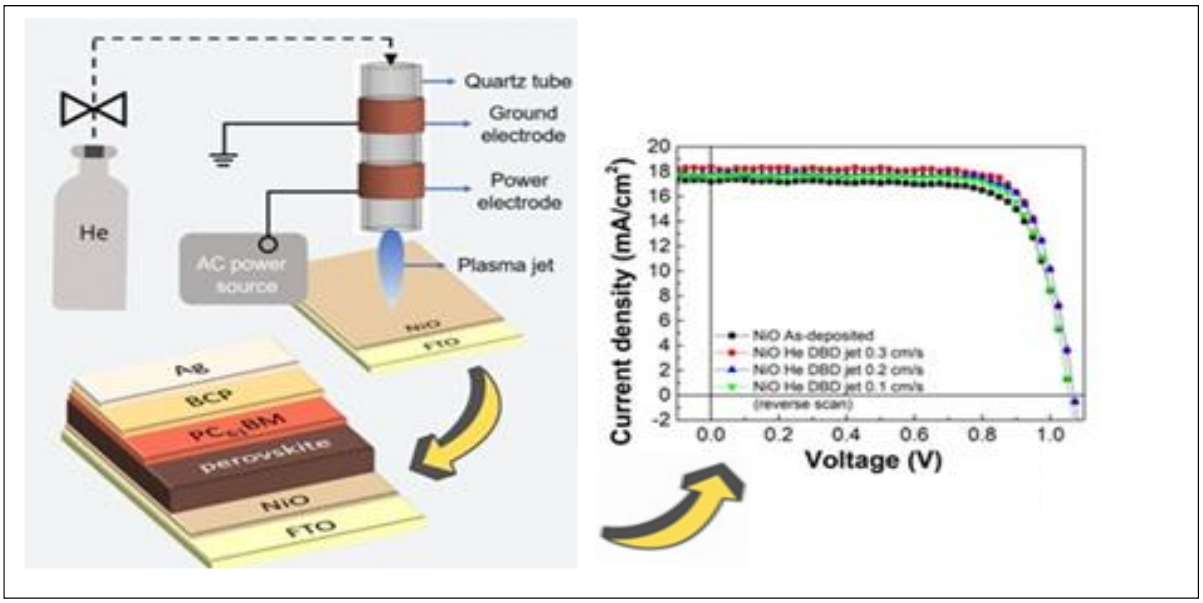

Figure 5: On the left side. Schematic of the dielectric-barrier-discharge-jet (DBDjet) helium plasma treatment. On the right side, the J-V curves characteristics of the p.i.n PSCs incorporating the NiO_x films treated with DBDjet process. Reprinted from ref 63. Copyright 2020 American Chemical Society.

Table 1: Device structures and photovoltaic parameters of the PSCs with physically treated NiO_x.

	Device Configuration	**V_{OC} (V)**	**J_{SC} (mA cm^{-2})**	**FF (%)**	**η (%)**	**Physical Treatment**	**Ref.**
1	ITO/NiO_x/$MAPbI_3$/PCBM/AZO/Ag	1.04	21.2	68	14.8	O_2 plasma (3min)	[61]
2	FTO/NiO_x/$MAPbI_3$/PCBM/BCP/Ag	1.11	23.41	75.18	19.67	UVO (5min)	[19]
3	ITO/ NiO_x/ $MA_{0.65}FA_{0.35}PbI_3$/ PCBM/BCP/Ag	1.04	23.17	78.8	19.15	O_2 plasma (2 min)	[62]
4	FTO/NiO_x/$MAPbI_3$/PCBM/BCP/Ag	1.07	18.23	76.19	14.88	He DBDjet 0.2 cm/s	[63]
5	ITO/ NiO_x/ $MAPbI_3$/ PCBM /LiF/Al	1.02	19.0	63	12.4	O_2 plasma (1 min)	[64]
6	ITO/ NiO_x/ $MAPbI_3$/ PCBM /BCP/Al	1.08	20.3	74.3	16.2	UVO (15min)	[65]

3. Surface modifications by chemical processes

Surface modifications by chemical processes are based either on the introduction of a thin interlayer of organic molecules or the chemical passivation of the NiO_x. Both these approaches are promising to simultaneously improve the surface morphology (leading to a better crystallization of the perovskite) and electrical properties of metal oxide thin films. Recent results based on this strategy are summarized in **Table 2**.

Different works have shown that Self-assembled monolayers (SAMs) can act as efficient interlayers to modify the surface properties between NiO_x and perovskite, leading to efficient hole extraction [66-75]. Indeed SAMs are thermodynamically ordered monolayers which typically consist of anchoring group (often called the head), linker (spacer), and functional groups (tail group) [76]. The anchoring group can easily bond with the surface while the spacer is a long alkyl chain connection with van der Waals interaction and the functional group works to alter the wettability of the upper layer, facilitating the deposition of the forthcoming layer by improving crystallinity, morphology, and energy level offset [49].

Lee et al., utilized tetramethylammonium hydroxide (TMAH) to significantly improve the interface between perovskite and NiO_x film prepared by sol-gel. The TMAH modification promoted a uniform and smoother surface, as the surface roughness was reduced from 7.4 nm to 0.6 nm. Moreover, the formation of nonstoichiometric Ni^{3+} components in nickel oxide crystals leads to desirable electrical properties. The modified NiO_x/perovskite interface improved the hole extraction, suppressed recombination, and improved the energy level alignment (ϕ ~ 5.42 eV) between the perovskite layer and NiO_x. The inverted planar PSC (ITO/NiO_x/$MAPbI_3$/ PCBM/C60/Ag) reported an improvement of PCE from 12.30 to 17.03% [66].

Q. Wang et al. used a series of benzoic acid SAMs (functional groups with NH_2, OCH_3, H, Cl, and Br) as interfaces between NiO_x and perovskites in an inverted PSCs configuration

(ITO/NiO_x/$MAPbI_3$/ PCBM/C60/Ag), **Figure 6**. The NiO_x NPs dispersed in water were prepared by spin coating onto the ITO-coated glass substrates with no further heating followed by SAM monolayer formation. The authors showed that SAM with a negative dipole moment decreases the

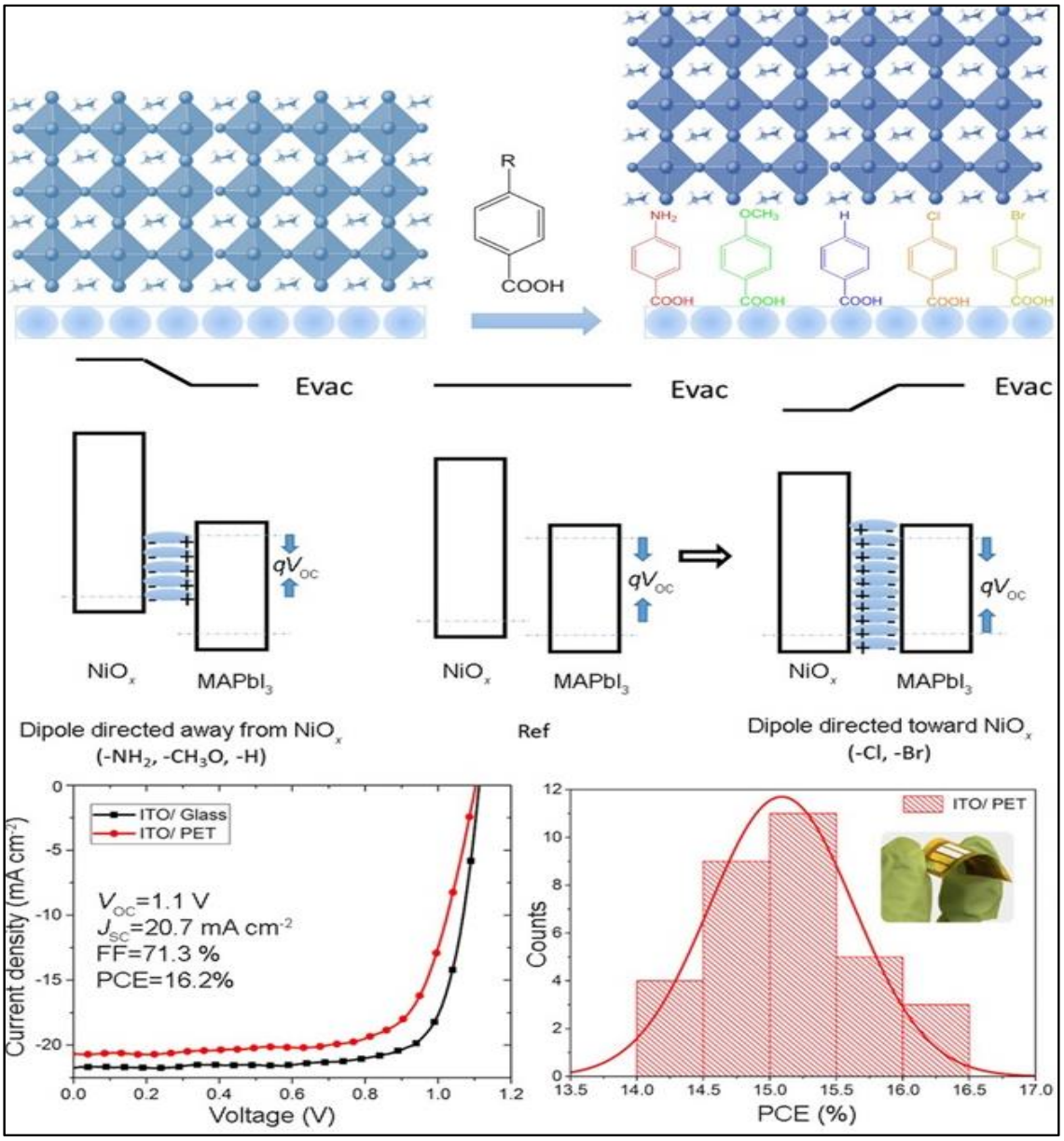

Figure 6: Top panel. Schematic diagram of the NiO_x/$MAPbI_3$ structure (left) and NiO_x/SAMs/$MAPbI_3$ structure (right) together with the schematic diagram of the band bending caused by the SAMs with different dipole moments. Middle panel. Quasi-Fermi levels are shown as dashed lines. Bottom panel. J-V curves of the Br-BA-modified PSCs made on glass substrates and F-PSCs made on flexible PET substrate and PCE distribution of the Br-BA modified F-PSCs over 32 devices Reprinted from ref 67. Copyright 2017 Wiley-VCH Verlag GmbH & Co. KGaA.

work function of the material. Br-BA SAM with positive dipole moments induces a band bending downward NiO_x/perovskite interface increasing the WF of NiO_x. Moreover, Br-BA SAM healed the NiO_x surface defects and enhanced the perovskite crystallization. The presence of the SAM enhanced the PCE from 15.5% to 18.4%. For the stability test, the PSCs were kept at 30% RH for 15 days. The reference PSCs maintained 70% of their original PCE, whereas the Br-BA-modified PSCs maintained about 80% of their original PCE. [67].

J. Zhang et al. show that the ferrocene dicarboxylic acid (FDA) SAM can modify both p-type and n-type carrier transporting layers. The authors modify a 20 nm thick sol-gel-processed NiO_x film with the SAM. The FDA-modified NiO_x shows a reduced roughness (from 8.01 nm to 5.57 nm) and higher hydrophobicity which guarantees the formation of larger perovskite grains. The high PL quenching of perovskite onto NiO_x/FDA shows that efficient charge transfer from the perovskite to the NiO_x layer using FDA. The PSC with a structure of ITO/NiO_x/$MAPbI_3$/PCBM/AgAl showed improved PCE from 15.13% to 18.20% when the SAM was introduced. Moreover, the NiO_x/FDA PSCs showed an improved UV resistance primarily attributed to the passivation effect of FDA and the better crystallization of the perovskite. The study shows that carboxyl groups (–COOH) can also passivate the perovskite layer [68]. Similarly, surface treatment with ethylphosphonic Acid, 4-Bromobenzoic Acid, Hexanoic acid, 4-bromobenzylphosphonic acid, etc showed to be efficient in improving the performances of NiO_x based PSCs [69-71].

Z. Li et al., also showed triphenylamine-imidazole derivatives with a different number of a methoxy group (TPI, TPI-2MEO, TPI-4MEO, TPI-6MEO) can act as HTL and surface modifiers simultaneously. Nitrogen and Oxygen atoms in TPI-6MEO forms Lewis adducts with undercoordinated Ni and Pb ions in NiO_x and perovskite leads bifacially passivation of those defect

sites and improving the crystallinity of perovskite. TPI-6MEO based PSCs show enhanced photovoltaic performances achieving a PCE of 18.42% in comparison to the reference device which had a PCE of 14.57%. The TPI-6MEO based PSCs device maintains 85% of its original PCE under UV light exposure for 21 h, while the reference device retained only 30% of its initial PCE [72].

W. Chen et al. proposed an alkali halide (NaCl, KCl) interfacial passivation of the NiO_x, which significantly improved the open-circuit voltage (V_{oc}) of the PSCs from 1.07 V to 1.15 V. This enhancement is attributed to increased grain size, good crystallinity of perovskite film as confirmed by XRD on KCl treated film. XPS data shows reduced adsorbed hydroxyl groups on the surface, which indicates a better-quality surface with fewer defects. Ab initio molecular dynamics study shows elimination of Pb-I antisites, heals the interface contact, which is probably caused by the interface structure ordering induced by NaCl. KCl-modified PSCs also maintained over 95% of initial performance after 150 d storage at nitrogen-filled dry box compared to pristine NiO_x (85%). The KCl-modified PSCs (ITO/NiO_x/$CsFAMAPbBrI_3$/PCBM/ZrAcac/Ag) show an improved PCE of 20.96% compared to one of the pristine PSC (18.92%), **Figure 7a** [73].

Similarly, T. Wang and co-workers studied the effects of an ultrathin sodium dodecylbenzene sulfonate (SDBS) film introduced between the perovskite and NiOx. The modification on the NiOx HTL by SDBS surfactant induced a better crystallinity of perovskite by regulating the wettability of the NiOx surface. The modified PSCs,(FTO/NiO_x/$MAPbI_3$/PCBM/BCP/Ag), show a PCE of 20.15%, in comparison with PCE of 16.26% for the reference PSC, **Figure 7b** [74].

Y. Du used a thin PTAA (poly(triaryl)amine) interlayer between the perovskite and NiO and controlling the wettability of the NiO_x surface and tailoring the perovskite grain size and crystallinity. The PTAA significantly facilitated interfacial charge transfer due to the gradient band

alignment and the PSCs showed an improved PCE of 17.1% as compared to the pristine NiO_x (13.2%) PSC [77].

Other important treatments such as PEDOT: PSS treated NiO have also been carried out. I. J. Park et al. demonstrated a hybrid PEDOT/NiO_x hole-extraction layer. The FF of the NiO_x-based perovskite solar cell can be significantly improved by treating the NiO_x surface with a dilute PEDOT solution (1 v/v % PEDOT/NiO_x). Photoluminescence quenching and impedance spectroscopic results show that hole injection at the perovskite/ NiO_x interface is significantly facilitated with the PEDOT treatment, results in increased FF. 1 v/v % PEDOT treated NiO_x device shows improved device performance without showing the hysteresis effect. (J_{sc} ~ 19.4 mA cm^{-2}, V_{oc} ~ 1.02 V, FF~ 0.70 and PCE ~ 13.9 %) compared with single NiO_x (J_{sc} ~ 18.9 mA cm^{-2}, V_{oc} ~ 1.03 V, FF~ 0.63 and PCE ~ 12.4 %) and PEDOT (J_{sc} ~ 17.1 mA cm^{-2}, V_{oc} ~ 0.92 V, FF~ 0.72 and PCE ~ 11.4 %) PSCs [78].

Similarly in 2020 Fan Wu et al. demonstrated PEDOT:PSS treated NiO_x PSCs with reduced hysteresis with an average hysteresis index of 0.020 as compared to single NiO_x device (0.142) or single PEDOT:PSS (0.093). PEDOT:PSS treated NiO_x PSCs show improved photovoltaic performances (J_{sc} ~ 23.78 mA cm^{-2}, V_{oc} ~ 0.97 V, FF~ 0.67 and PCE ~ 15.45 %) as compared with pure NiO_x (J_{sc} ~ 22.21 mA cm^{-2}, V_{oc} ~ 0.94 V, FF~ 0.60 and PCE ~ 12.53 %) and PEDOT:PSS (J_{sc} ~ 20.85 mA cm^{-2}, V_{oc} ~ 0.93 V, FF~ 0.77 and PCE ~ 14.93 %) PSCs [79].

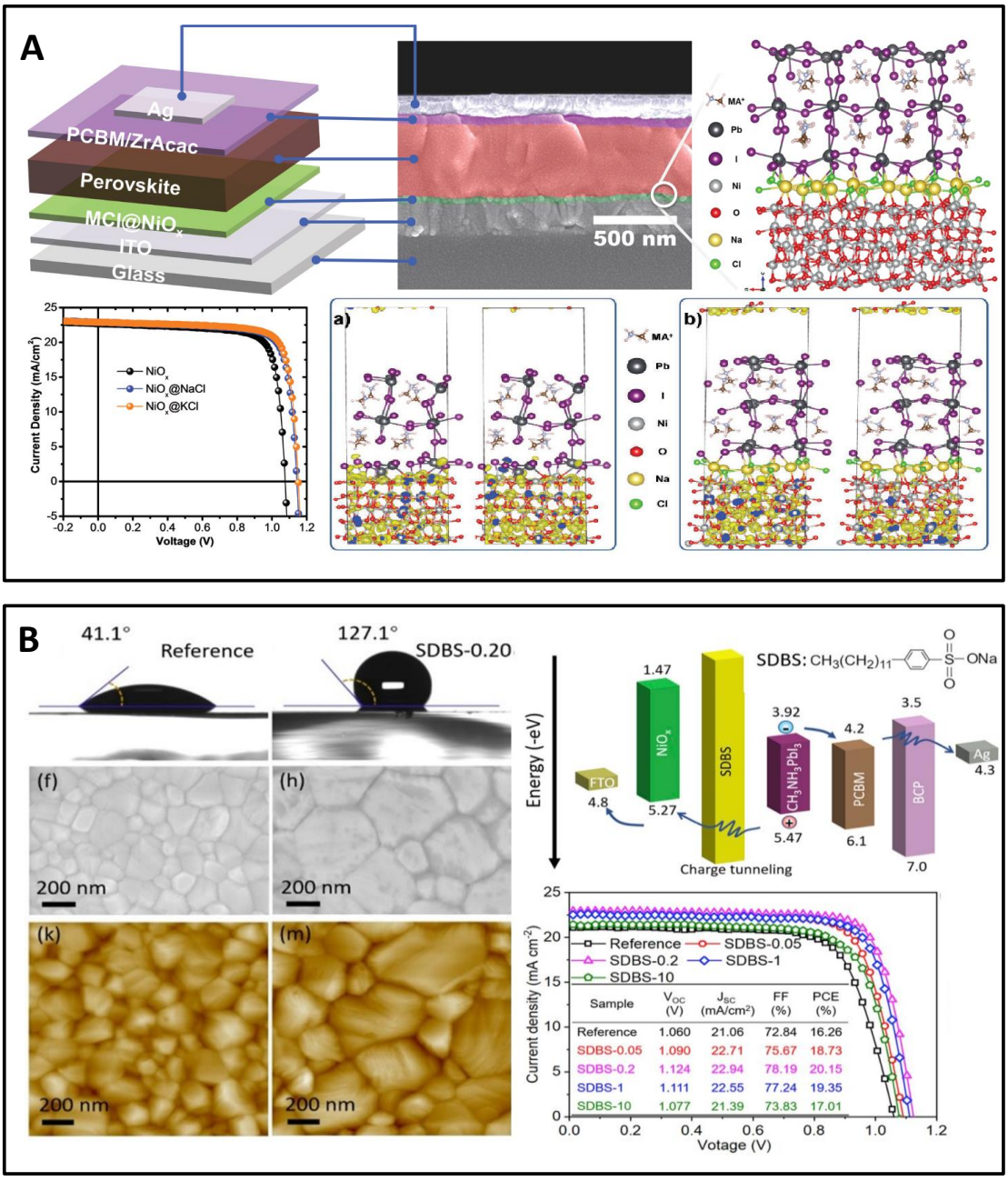

Figure 7: A. Schematic device architecture, cross-sectional SEM image and J-V curve of of PSCs with alkali chlorides (MCl) modified NiO_x as HTLs; A supercell illustrating the structural details in perovskite/NaCl/NiO_x HTL interface, Ab initio molecular dynamics (MD) of NiO-perovskite and NiO-NaCl-perovskite interfaces. (Reprinted from ref 73. Copyright 2019 Wiley-VCH Verlag GmbH & Co. KGaA) For simplifying the calculation, $MAPbI_3$ perovskite supercell was used for MD simulation. **B**. The contact angle of water, SEM, AFM images and J-V curve on the NiO_x/SDBS based PSCs with different concentrations of SDBS. (Reprinted from ref 74. Copyright 2020 Elsevier)

Table 2: Device structures and photovoltaic parameters of the PSCs with chemical treated NiO_x

	Device Configuration	**V_{OC} (V)**	**J_{SC} (mA cm^{-2})**	**FF**	**η (%)**	**SAM**	**Ref.**
1	ITO/NiO_x /MAPbI3/PCBM/C60/Ag	1.11	21.7	76.3	18.4	Br-benzoic acid, (0.1cm^2)	[67]
2	ITO/NiO_x/ $MA_{0.65}FA_{0.35}PbI_3$/ PCBM/BCP/Ag	1.04	23.2	76.1	18.7	post-annealing, O_2-plasma, and potassium chloride treatments (0.1 cm^2)	[62]
3	ITO/NiO_x/ $MAPbI_3$/ PCBM/C60/Ag	1.08	21.90	72	17.03	Tetramethylammonium hydroxide (TMAH, 0.1cm^2)	[66]
4	ITO/ NiO_x/ $MAPbI_3$/ PCBM/BCP/Ag	1.07	21.90	81	18.9	Thermally reduced graphene oxide NiO_x:rGO (2 vol%)	[80]
5	ITO/NiO_x/ $FAMAPbI_3$/ PCBM/BCP/Ag	1.05	18.5	70	13.0	Ethylphosphonic Acid	[69]
6	ITO/NiO_x/ $FAMAPbI_3$/ PCBM/BCP/Ag	1.01	19.8	64	12.6	4-Bromobenzoic Acid	[69]
7	FTO/ $SrNiO_x$ PEAI/$MAPbI_3$/PCBM/AgAl	1.09	24.27	76.55	20.31	Phenethyl ammonium iodide (PEAI)	[75]
8	ITO/NiO_x/CsBr/$MAFAPbI_3Cl$/PCBM/BCP/Ag	1.09	23.5	75.1	19.2	CsBr-2.5	[81]
9	FTO/TiO_2/$CsMAFAPbI_3C$/NiO_x /Au	0.99	21.9	60	13.1	Hexanoic acid (HA)	[70]
10	ITO/NiO_x/$MAPbI_3$/PCBM/AgAl	1.04	22.55	76.2	18.20	Ferrocenedicarboxylic acid (FDA)	[68]
11	ITO/NiO_x/$CsFAMAPbBr_3I_3$/PCBM/Ag	1.09	18.58	67.18	12.73	4-bromobenzylphosphonic acid	[71]
12	ITO/NiO_x/$MAPbI_3$/PCBM/BCP/ Ag	1.03	20.35	72.09	15.25	glycerol/choline chloride (1:1/m:m)	[82]
13	ITO/NiO_x/TPI-6MEO/$MAPbI_3$/PCBM/BCP/Ag	0.98	23.31	81	18.42	triphenylamine-imidazole (TPI-6MEO)	[72]
14	ITO/NiO_x/$CsFAMAPbBrI_3$/PCBM/ ZrAcac/Ag	1.15	22.89	79.3	20.96	KCl	[73]
15	ITO/NiO_x/$CsFAMAPbBrI_3$/PCBM/ ZrAcac/Ag	1.14	22.83	79.6	20.71	Nacl	[73]
16	FTO/NiO_x/$MAPbI_3$/PCBM/BCP/ Ag	1.12	22.94	78.19	20.15	sodium dodecyl benzene sulfonate (SDBS)	[74]
17	FTO/NiO_x/$MAPbI_3$/PCBM/BCP/ Ag	1.11	20.70	79	18.03	Li-bis-(trifluoromethanesulfonyl) imide, Li-TFSI	[83]
18	FTO/NiO_x/$MAPbI_3$/C60/BCP/Ag	1.08	22.8	77.9	18.9	n-Butylamine	[84]

4. Elemental Doping

NiO has a highly stable ionic crystal structure with a high melting point. [38, 50, 85]. Ultrathin NiO film with thickness comparable to the characteristic length of the space charge region (Debye length) result high electrical conductivity with high optical transparency[38] while slightly thicker (few nanometers) NiO layer result to be intrinsically insulators. Most of the NiOx films used as ELT have a thickness 7–20 nm [36, 86-88] resulting to be intrinsically insulators and require doping strategies to improve the p-type conductivity by can reducing the trap states and modify the work function [80]. Dopants as transition metals (*i.e.*: Cu, Ag, Co, Zn, etc.,), alkali/alkaline-earth metal (*i.e.*: Li, Mg, Sr, etc.), and/or their combination to the large ionic radii difference [89] can introduce lattice distortion/defects in the NiO_x matrix and affecting the carrier mobility and optical transmittance [90]. Therefore, the selection of dopants and optimization of their doping levels in the NiO matrix for high-performance PSCs is critical. Different doping strategies in NiO_x films and their effect on the performance of the PSC_s are summarized in **Table 3**

Copper (Cu) is the best doping element in NiO_x HTL as Cu and Ni have the same crystal structure (fcc), same valence (+1), similar atomic radii (size mismatch ~ 2%), and similar electronegativity (difference ~ 2%). The Cu shows complete solid solubility in nickel [91]. The substitution of nickel (Ni^{2+}) or the creation of acceptor-like native defects such as nickel vacancies by copper (Cu^{+} and/or Cu^{2+}) doping in NiO films can increase the carrier concentration. For example, the substitution of Ni^{2+} by a divalent copper (Cu^{2+}) would form an acceptor-like defect of nickel vacancy (V_{Ni}^{2-}) which increases the density of holes (h^{+}) However, the creation of such defects would result in a reduction of mobility. [92-96].

W. Chen et. al. prepared Cu-doped NiO (Cu:NiO) nanoparticle ink with a low doping level of copper (5.3 %) and fabricated good quality pinhole-free Cu:NiO films (thickness ~ 50 nm) by

spin-coating. They observed that the Cu:NiO film exhibited good crystallinity/pure phase(s) (**Figure 8a**) with a small change of interplanar spacing (d) of the crystal lattice as confirmed from high-resolution transmission electron microscopy (TEM) images and [97] increased conductivity due to the substitution of Ni^{2+} by Cu^{+} [98]. Besides, the copper doping forms a shallower acceptor level (~0.7 eV just above the Fermi level) than the nickel vacancies (~ 1.3-2.0 eV above the Fermi level) of bulk NiO. This increased conductivity and work function (5.25 eV). The Cu:NiO was utilized as HTL in rigid and flexible PSCs achieving respectively PCEs of ~20.26% and ~17.41%, **Figure 8a**. The encapsulated PSCs exhibited negligible hysteresis and also maintaining ~ 95% of initial PCE when stored in ambient at 50–65% humidity for 1000 h. [97]. Further, R. Ishikawa and co-workers showed that Ag^{+} doping in NiO is effective due to its stable valence of +1 (M^{+1}) to improve the conductivity. However, its large ionic radius of ~ 1.15Å can substitute only a small amount of Ni^{2+} which has an ionic radius of ~ 0.69 Å. The concentration of Ag in NiO_x largely affects the optoelectronic properties of the NiO_x films. It has been reported that small Ag^{+} doping (~ 1.8 at%) in NiOx increased significantly the conductivity (1.1×10^{-1} S/cm) with almost no changes in the hole mobility (0.09 cm^2/Vs) while using larger Ag^{+} amounts (13.1 at.%) in NiO_x degraded the hole mobility and optical transmittance [99]. In this work, they employed the NiO_x doped films in CdTe solar cells.

J. Zheng and his co-workers showed that an Ag-doping at 3.6 at.% in NiO_x, as compared to a pure NiO_x film, improved the electrical conductivity (from $\sigma = 6.6\times10^{-7}$ S/cm to $\sigma = 2.2\times10^{-6}$ S/cm), the work function (from, ~5.02 eV to ~ 5.13 eV), and the morphology (root mean square roughness, R_{rms}, went from ~ 7.1 nm to ~ 6.0 nm) while maintaining a comparable optical average transmittance (T_{av} ~82%). The Ag-doping in NiO increases hole concentration via an increase in oxygen vacancies as following [100].

$$2NiO \rightarrow V_{Ni}^{2-} + 2h^{+} + 2O_{O}^{x} + Ni_{surface}^{x} \quad (1)$$

$$2NiO \xrightarrow{0.5Ag2O} Ag_{Ni}^{-} + V_{Ni}^{2-} + 3h^{+} + 2.5O_{o}^{x} + Ni_{surface}^{x} \quad (2)$$

where V_{Ni}^{2-} represents the Ni cation vacancy at the intrinsic Ni site, h^{+}represents a hole, O_{O}^{x} is the normal oxygen at intrinsic oxygen site, $Ni_{surface}^{x}$ is the Ni atom at the surface site, and Ag_{Ni}^{-} is the Ag cation vacancy at the intrinsic Ni site. The Ag (3.6 at. %) doped NiO_x HTL was integrated into PSCs with the ITO/Ag: NiO_x/$CH_3NH_3PbI_3$/PCBM/BCP/Ag structure and PCE of 17.3% were achieved while the undoped NiO_x based PSCs had a PCE ~ 15.7%.

Few works have also demonstrated the effectiveness of transition metals such as cobalt (p-type dopant, ionic radius ~ 0.745 Å) and zinc (n-type dopant, ionic radius ~ 0.74 Å), in improving the optoelectronic properties of NiO HTLs [101-104].

Y. Xie and his coworkers demonstrated a NiO HTLs film with a 6 mol% doping of cobalt with significantly improved optoelectronic properties as compared to the pristine NiO: the work function was Φ ~ -5.20 eV vs the Φ~ -5.12 eV and electrical conductivity, σ ~2.5×10^{-3} S/cm to σ = 4.4×10^{-5} S/cm respectively. The films were incorporated into inverted PSCs achieving higher PCEs of ~ 18.6% , over 2% higher than the value of the PSCs which employ pristine NiO_x [101].

Recently, Lee et. al., developed near infra-red annealed cobalt doped NiO_x (NIR-Co:NiO_x) HTLs with optimum cobalt doping of ~ 4 mol% with enhanced mobility (0.21 cm^2/Vs), leading to reduced charge recombination and enhanced hole extraction rate [102] to replace the pristine NiO_x HTLs in PSCs. The PSCs integrating the NIR-Co:NiO_x HTL showed a PCEs of ~17.77%, significantly higher than the ones of the PSCs using pristine NiO_x HTL (~15.99%).

X. Wan et al. showed that Zinc (ionic radius ~ 0.74 Å) doping in NiO_x reduces the ionization energy of nickel vacancies and allows the formation of a film with compact and smooth (R_{rms} ~ 2.61 nm) morphology, leading to a continuous and smooth perovskite layer. Interestingly, the zinc-

doped NiO_x film (with 5 mol%) exhibited higher work function (5.3 eV) and electrical conductivity (high current showed by conductive AFM) and similar transparency (95%) to the pristine NiO_x. PSCs based on zinc-doped NiO_x achieved high remarkable efficiency of 19.6% with negligible hysteresis, **Figure 8b** [103]. W. Chen et al. showed that similarly to the zinc (n-type dopant) doping, alkali metal ions viz., lithium (Li+) and cesium (Cs+) ions can also substitute the nickel in NiO_x lattice to enhance the conductivity without degrading the visible transmittance [105]. A combinational doping approach of Li or Cs with p-type dopants of transition metal (such as Cu, Ag, Co) in NiO_x has also been demonstrated to be efficient in maintaining a high transmittance and improve the electrical characteristics and resulting high performing PSCs, **Table 3** [104, 106]. G. Li et al. showed that a large amount of Mg (8 at. %) in NiO_x can substitute the nickel but it increases the conductivity by only one order from 0.67×10^{-6} S/cm to 0.27×10^{-5} S/cm. In contrast to the Li and Cu doping in NiO_x, the Mg doping resulted in a slightly higher transmittance in the shorter wavelength of the visible region (<500 nm) than the NiO_x. The $NiMgO_x$ with Mg content of 8 at.% was used as an HTL in PSC with a PCE of 18.5% high ambient stability [107]. On the other hand, W. Chen et al. showed that elements with similar ionic radii as Mg^{2+} (0.71Å), Li^{+} (0.76Å), and Ni^{2+} (0.69Å) can form High-quality $Li_{0.05}Mg_{1.5}Ni_{0.8}O$ ternary oxide via Mg and Li co-doping in NiO_x. The film prepared by spray pyrolysis has been integrated as an HTL in $MAPbI_3$ based PSC which achieved a certified PCE of 15.0% for a 1.017 cm^2 active area [108].

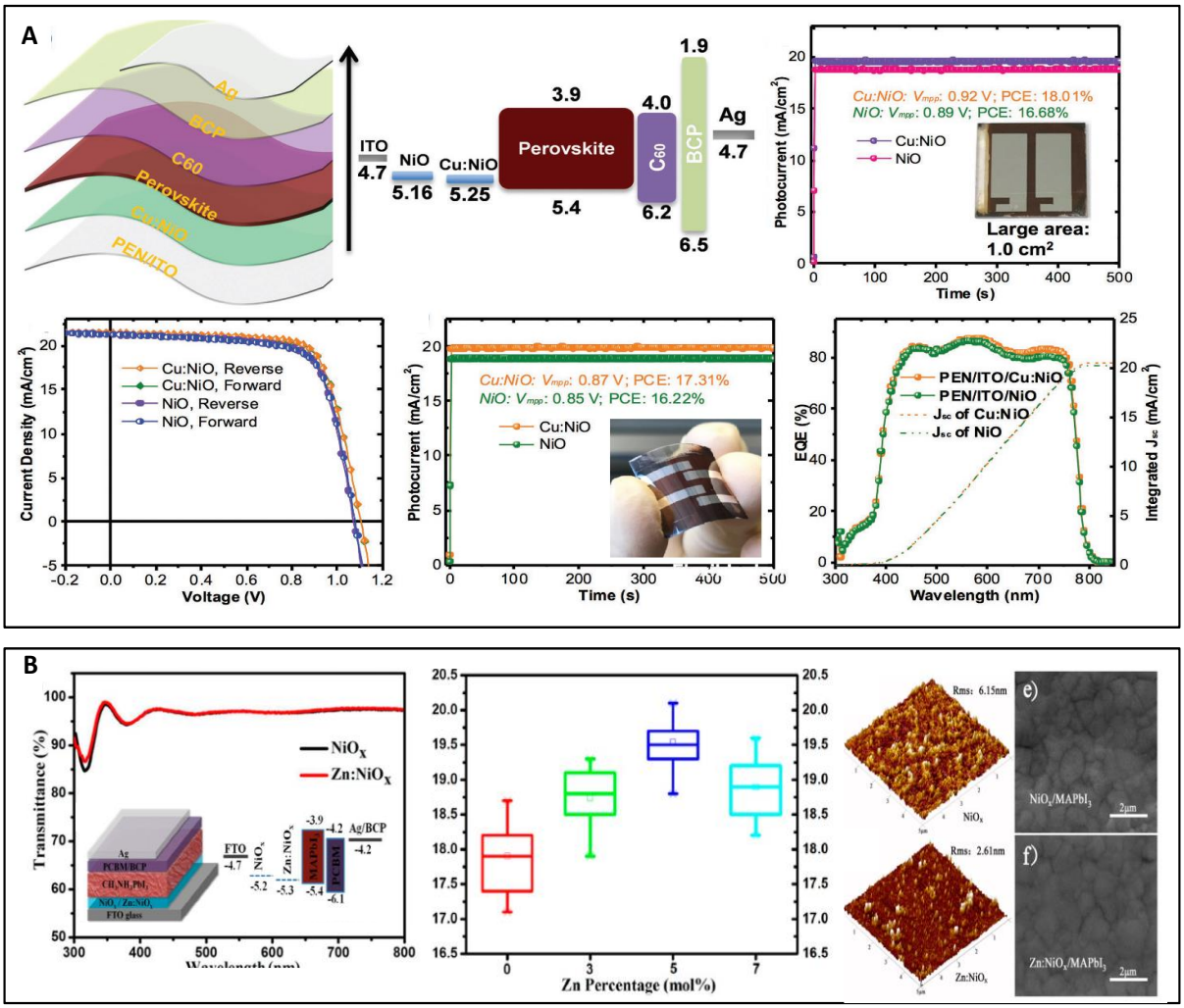

Figure 8: **A.** Structural illustration of the inverted planar PSCs. Top panel. Schematic diagram of energy levels at the inverted PSCs, steady photocurrent output at fixed applied voltage (V_{mmp}) over 500 s, inset shows a photograph of large-area device. Bottom panel. I-V curves of the optimal flexible PSCs, steady photocurrent output as function of applied time (500 s) and EQE spectra of the optimal flexible PSCs based on NiO and Cu:NiO HTLs. Reprinted from ref 97. Copyright 2018 Wiley. **B.** Transmittance spectra of the NiO_x and NiO_x:Zn films coated on glass substrates (inset showing device architecture and energy band diagram of of the inverted planar PSC, PCE histogram of devices with different zinc concentration. 3D-AFM and SEM images of the corresponding NiOx and NiOx:Zn films. Reprinted from ref 103. Copyright 2018 American Chemical Society**.**

X. Chen et al. prepared NiO_x films doped with various rare earth elements (Ce, Nd, Eu, Tb, and Yb) by solution method and systematically studied the impact of various dopants and their concentration on the structure and optoelectronic properties of the NiO_x. Also, low doping (up to 3%) in NiO_x resulted in a film with a smooth and compact structure with higher carrier

concentration and mobility, especially, for the 3% Eu: NiO_x film. The inverted PSCs using 3% Eu: NiO_x displayed a PCE of 15.06% [109-110]. This was mainly attributed from the increased short circuit current density values due to the smaller series resistance values and the improved conductivity [110]. A larger amount of yttrium doping (5 mol%) in NiO_x was possible due to the smaller ionic radius as compared with the radii of other rare earth elements. The 5%Y-NiO film showed a compact morphology, high hole mobility, and good charge extraction efficiency. The PSC using 5%Y-NiOx film as HTL exhibited a PCE of 16.31 % as compared to the 11.80 of PSCs incorporating the pristine film. [111].

Table 3: Device structures and photovoltaic parameters of the PSCs including co-doped NiO_x as HTL.

	Device Configuration	**V_{OC} (V)**	**J_{SC} (mA cm^{-2})**	**FF**	**PCE (%)**	**Dopant (%)**	**Ref.**
1	FTO/NiO_x/$MAPBI_3$/PCBM/Au	1.00	23.82	68	16.31	5%Y (yttrium)	[111]
2	FTO/NiOx/$FAMAPb(BrI)_3$/PCBM/AgAl	1.11	22.68	79.1	20.07	1 at.% Sr (Strontium)	[112]
3	ITO/NiOx/$MAPBI_3Cl_{3-x}$/PCBM/Al	1.12	21.79	73.6	18	Li (Lithium)	[113]
4	FTO/NiO_x/$MAPBI_3$/PCBM/Au	1.13	21.29	80	19.24	Li (0.5 at. %), Ag (1.5 at.%) (Lithium Silver co-doped)	[106]
5	ITO/NiO_x/$MAPBI_3$/PCBM/Al	1.05	22.3	79	18.6	6% mol Co (Cobalt)	[101]
6	ITO/NiO_x/$MAPBI_3$/PCBM/BCP/Ag PET/ NiO_x/$MAPBI_3$/PCBM/BCP/Ag	1.08 1.09	19.16 18.16	84.81 72.44	17.57 14.42	1.0 mol% Fe (flexible)	[42]
7	ITO/NiOx/MAPbI3/C60/Ag	1.05	22.23	76	17.74	Cu (Copper)	[114]
8	FTO/NiO/MAPbI3/PCBM/BCP/Ag	1.1	22.8	78	19.6	5 mol % Zn (Zinc)	[103]
9	ITO/NiO_x/$MAPBI_3$/PCBM/ZnMgO/Al	21.3	79	79	18.2	8 at% Mg (Magnesium)	[107]
10	FTO/NiOx/$CsFAMAPb(IBr)_3$/PCBM+TBABF4/TIPD/Ag	1.13	20.05	74	17.05	3 mol% K (Potassium)	[115]
11	ITO/NiO_x/$FAMAPB(ClI)_3$/PCBM/BCP/Ag	1.09	23.8	78	20.1	10 mol % (Li) ,5 mol % (Co)	[104]
12	ITO/NiOx/MAPbI3/PCBM/BCP/ Ag	1.06	20.4	74.7	16.3	5 mol% Ag (silver)	[100]
13	FTO/ NIR Co:NiOX/MAPbI3/PC61BM/PEI/Ag	1.09	20.46	79.80	17.77	NIR- 4 mol % Co:NiO_X	[102]
14	FTO/NiOx/MAPbI3/PCBM/ZrAcac/Ag	1.11	21.79	79.5	19.29	1 mol% Cs (cesium)	[105]
15	FTO/NiO/MAPbIBr/PCBM:C60/BCP/Ag	1.01	22.59	77.98	17.81	3vol% K (Potassium)	[116]
16	FTO/BL-NiOx/MAPbI3/PCBM/BisC60/ Ag	1.11	21.58	81.9	19.62	Bilayer Cu:NiOx/mpCu:NiO	[117]
17	ITO/NiOx/MAPbI3/C60/BCP/ Ag PET/ NiO_x/$MAPBI_3$/C60/BCP/Ag	1.12 1.10	22.23 21.24	80.9 73.5	20.15 17.26	Rigid Flexible ,Cu	[97]

4.1 Chemical treatment on co-doped NiO

To further improve the V_{oc} and hence the performance of the NiO-based p-i-n devices, a variety of chemical treatments have been applied on the metal-doped NiO_x films to reduce the defect states between the doped NiO_x and perovskite layer.

J. He et al. prepared highly crystalline Cu:NiO_x thin films and studied their photophysical properties after surface modification by three small molecules: glycine (Gly), cysteine (Cys), and mercaptoethylamine (Merc) chlorate, **Figure 9a**. The Cu:NiO_x surface exhibits a high contact angle of 96°. The surfaces modified by Cys and Merc molecules resulted to have lower contact angle values of 81° and 67°, respectively. The Cys molecule has an extra carboxyl group than the Merc. The Cu: NiO_x surface treated with Cys exhibited a higher work function than the Merc treated film due to the high electrophilicity ability of the carboxyl group. The Cu: NiO_x surface attached with Cys or Merc enhanced the preferential orientation of the perovskite layer overlaid on it and improved the red-light harvesting and charge transfer properties of the perovskite film. The PSCs with Cu:NiO_x/Cys modification, as compared to the untreated one report improved short circuit current density from 20 to 23.6 mA cm-2 and open-circuit voltage (from 1.06 to 1.12 V) reaching shows PCE over 18% [118].

Y. Zhang et al., prepared p-NiMgLiO thin film (thickness ~ 20 nm) by spray pyrolysis and treated them with an organic monolayer made of bifunctional 5-aminovaleric acid (5-AVA) molecules. The 5-AVA molecules were completely absorbed onto the NiMgLiO's surface as confirmed from the Fourier Transform Infrared (FTIR) analysis, **Figure 9b**. The carboxyl functional group of the 5-AVA molecules easily attached to the NiMgLiO surface and improved its wetting characteristics, while the amino functional group of the 5-AVA molecules strongly coordinated

with the perovskite layer increasing the crystallinity. The treated PSCs achieved an improved PCE of 19.4% as compared to the 18.0% achieved by the reference device [119].

Similarly, Y. Liu et al., explored the Phenethyl ammonium iodide (PEAI) to passivate the Sr doped NiO_x films. The PEAI attached with SrNiOx surface reacts with $MAPbI_3$ perovskite layer deposited on top to form quasi-2D PEA_2PbI_4 grains at the SrNiOx/perovskite interface. The quasi-2D PEA_2PbI_4 perovskite layer exhibits higher conduction band energy and can block electron transport into the p-type SrNiOx interface, limits carrier recombination at the interface. In addition, the hydrophobic organic cation (PEA+) with a benzene ring of the PEAI improves the moisture resistance of interfaces. The PEAI modified SrNiOx film leads to improve the crystallinity of the perovskite layer that showed larger grains elongated in the longitudinal direction as confirmed from the cross-sectional SEM images, **Figure 9c**. The PEAI coated on the SrNiOx filled up the pinhole defects and resulted in smooth and compact morphology of the perovskite layer. Therefore, the better quality of the perovskite layer, passivating interface defects, and adjusting the interface contact barrier after PEAI modification leads to reduce carrier recombination, facilitating carrier extraction and transport. Moreover, the stability of un encapsulated pure and with PEAI treated PSCs maintained 75% of the original PCE values, as compared to (47%) of the reference PSCs after aging for 10 h at 85 °C. The light stability of the PSCs was tested with a moderate illumination intensity of 42 mW/cm^2 at 50% RH showing that the PEAI modified PSCs maintained 65% of the original PCE values compared to 60% of the reference PSCs after aging for 240 h. These results indicate that devices with PEAI modification show better moisture resistance and superior thermal stability [75].

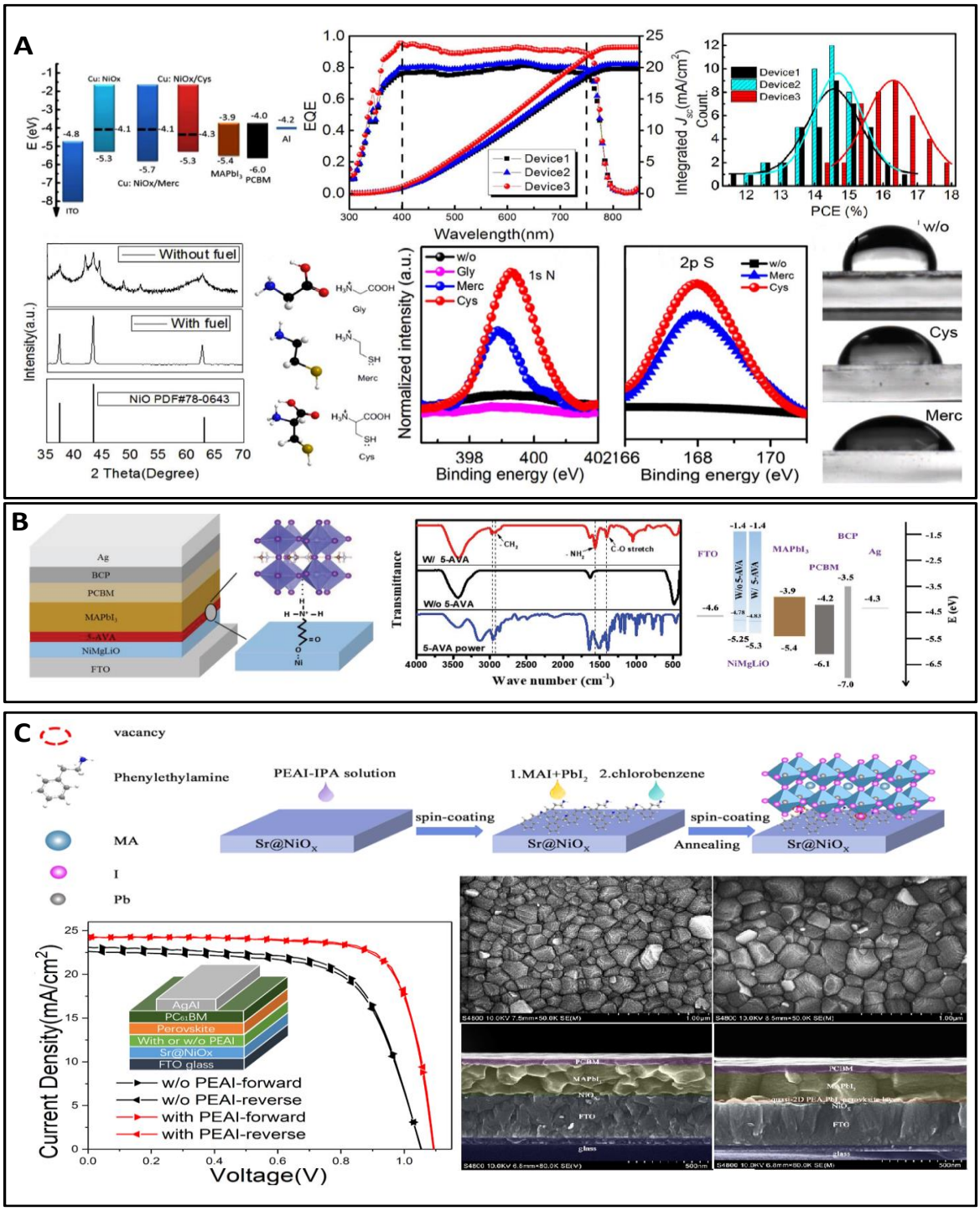

Figure 9: **A** From left to right: Schematic energy levels of the PSCs interlayers. The Fermi levels of bare Cu: NiO_x, Cu: NiO_x/Merc and NiO_x/Cys are represented by dashed lines. EQE spectrum and the the integrated short-circuit current density (J_{SC}). PCE distributions for Device1–3. Below: XRD of Cu:NiO_x prepared by precursor with or without fuel. Molecular 3D models and formula of three amino acids. XPS signals of N1s and S2p from surface of Cu:NiOx treated with different solution. Contact angle of the modified materials. (Reprinted from ref 118. Copyright 2018 Elsevier). **B.** Schematic diagram of the inverted PSC, highlighting the 5-AVA modified interface between NiMgLiO and $MAPbI_3$., FI-IR spectra of 5-AVA and NiMgLiO films with (W/) and without (W/o) 5-AVA modification, Schematic energy levels of the PSCs interlayer. Fermi levels of the NiMgLiO films with and without 5-AVA are denoted by the dashed lines. (Reprinted from ref 119. Copyright 2018 Wiley) **C** Schematic diagram of the PEAI-modified interface procedure. Below: J−V characteristics of PSCs without and with PEAI modification with a scanning rate of 100 mV/s. Top-view and Cross-sectional SEM images of perovskite films without and with PEAI modification. (Reprinted from ref 75. Copyright 2019 American Chemical Society).

5. Conclusion and outlook

In this review, we have discussed the impact of different physical and chemical surface modifications and doping approaches on NiO_x thin films to enhance the film conductivity and to improve the energy level alignment with metal halide perovskites and their subsequent effects on the performance and stability of inverted PSCs.

We highlighted that for the physical processes, UV-ozone treatments generated oxygen-rich stoichiometry and nickel oxyhydroxide (NiOOH) type-dipolar species which improved the conductivity and enlarged the work function of the NiO film, leading to photovoltaic improvements in the p-i-n PSCs. Similarly, the oxygen plasma is a suitable method to improve the work function and suppress the recombination at the perovskite/NiO_x interface.

Chemical modifications, based on the insertion of thin organic interlayers between the NiOx films and the perovskite have demonstrated potential in improving the charge transport in NiO_x. SAMs have been employed to induce the downward band bending and passivate the surface defects of both NiO_x and perovskite layer, leading to enhanced perovskite crystallization and improved interfacial contact.

Another approach to improve the conductivity of the NiO_x is based on the use of dopants. Various dopants and co-dopants of transition metals (Cu, Ag, Co, Zn, etc.,), alkali/alkaline-earth metal (Li, Mg, Sr, etc.) and/or combination of both metals (Cu-Li, Mg-Li, etc.,) and rare-earth elements (Y, La) in NiO_x have been explored to improve the film quality, work function, and optoelectronics characteristics the NiO_x films.

ALD, electron beam deposition and radiofrequency magnetron sputtering seem to be the best approaches to deposit high-quality NiO_x over a large area and keeping the substrate temperatures low with a reduced defect density [21, 32-33, 38-39, 120].

Moreover, targeting efficient and stable PSCs, the insertion of passivation layers is extremely important to passivate the NiO_x defects, adjusting the work function and enhancing the formation of high-quality perovskite films.

Overall, NiO_x based PSCs have now reached PCEs above 20%, together with low cost, easy processing, and long-term stability. The surface modifications and interlayers seem to be a strategical approach to further enhance their photovoltaic performances.

Notes

Two of the authors N.M. and S.M. are directors of Prominence Photovoltaics Pte Ltd a perovskite solar cell commercialization company. The other authors have no conflict of interest to declare.

Acknowledgments

This research is supported by the National Research Foundation, Prime Ministers Office, Singapore under the Solar CRP (S18-1176-SCRP) and NRF2018-ITC001-001

References

[1] A. Kojima, K. Teshima, Y. Shirai, T. Miyasaka, *J. Am. Chem. Soc.* **2009**, *131*, 6050.

[2] J. Jeong, M. Kim, J. Seo, H. Lu, P. Ahlawat, A. Mishra, Y. Yang, M. A. Hope, F. T. Eickemeyer, M. Kim, Y. J. Yoon, I. W. Choi, B. P. Darwich, S. J. Choi, Y. Jo, J. H. Lee, B. Walker, S. M. Zakeeruddin, L. Emsley, U. Rothlisberger, A. Hagfeldt, D. S. Kim, M. Grätzel, J. Y. Kim, *Nature* **2021**, *592*, 381.

[3] W. S. Yang, B.-W. Park, E. H. Jung, N. J. Jeon, Y. C. Kim, D. U. Lee, S. S. Shin, J. Seo, E. K. Kim, J. H. Noh, *Science* **2017**, *356*, 1376.

[4] W. S. Yang, J. H. Noh, N. J. Jeon, Y. C. Kim, S. Ryu, J. Seo, S. I. Seok, *Science* **2015**, *348*, 1234.

[5] F. Sahli, J. Werner, B. A. Kamino, M. Bräuninger, R. Monnard, B. Paviet-Salomon, L. Barraud, L. Ding, J. J. D. Leon, D. Sacchetto, *Nat. Mater.* **2018**, *17*, 820.

[6] J. Li, H. Wang, X. Y. Chin, H. A. Dewi, K. Vergeer, T. W. Goh, J. W. M. Lim, J. H. Lew, K. P. Loh, C. Soci, T. C. Sum, H. J. Bolink, N. Mathews, S. Mhaisalkar, A. Bruno, *Joule* **2020**, *4*, 1035.

[7] J. Li, H. A. Dewi, H. Wang, J. H. Lew, N. Mathews, S. Mhaisalkar, A. Bruno, *Sol. RRL* **2020**, *4*, 2000473.

[8] T. Liu, K. Chen, Q. Hu, R. Zhu, Q. Gong, *Adv. Energy Mater.* **2016**, *6*, 1600457.

[9] P.-K. Kung, M.-H. Li, P.-Y. Lin, Y.-H. Chiang, C.-R. Chan, T.-F. Guo, P. Chen, *Adv. Mater. Interfaces* **2018**, *5*, 1800882.

[10] Z.-L. Tseng, L.-C. Chen, C.-H. Chiang, S.-H. Chang, C.-C. Chen, C.-G. Wu, *Sol. Energy* **2016**, *139*, 484.

[11] J. Liu, S. K. Pathak, N. Sakai, R. Sheng, S. Bai, Z. Wang, H. J. Snaith, *Adv. Mater. Interfaces* **2016**, *3*, 1600571.

[12] P. Nazari, F. Ansari, B. Abdollahi Nejand, V. Ahmadi, M. Payandeh, M. Salavati-Niasari, *J. Phys. Chem. C* **2017**, *121*, 21935.

[13] H. S. Jung, N. G. Park, *small* **2015**, *11*, 10.

[14] N. Arora, M. I. Dar, A. Hinderhofer, N. Pellet, F. Schreiber, S. M. Zakeeruddin, M. Grätzel, *Science* **2017**, *358*, 768.

[15] J. A. Christians, R. C. Fung, P. V. Kamat, *J. Am. Chem. Soc.* **2014**, *136*, 758.

[16] P. K. Kung, M. H. Li, P. Y. Lin, Y. H. Chiang, C. R. Chan, T. F. Guo, P. Chen, *Adv. Mater. Interfaces* **2018**, *5*, 1800882.

[17] A. Bashir, S. Shukla, J. H. Lew, S. Shukla, A. Bruno, D. Gupta, T. Baikie, R. Patidar, Z. Akhter, A. Priyadarshi, *Nanoscale* **2018**, *10*, 2341.

[18] W. Chen, G. Pang, Y. Zhou, Y. Sun, F.-Z. Liu, R. Chen, S. Chen, A. B. Djurišić, Z. He, *J. Mater. Chem. A* **2020**, *8*, 1865.

[19] T. Wang, D. Ding, H. Zheng, X. Wang, J. Wang, H. Liu, W. Shen, *Sol. RRL* **2019**, *3*, 1900045.

[20] J. Troughton, K. Hooper, T. M. Watson, *Nano Energy* **2017**, *39*, 60.

[21] T. Abzieher, S. Moghadamzadeh, F. Schackmar, H. Eggers, F. Sutterlüti, A. Farooq, D. Kojda, K. Habicht, R. Schmager, A. Mertens, R. Azmi, L. Klohr, J. A. Schwenzer, M. Hetterich, U. Lemmer, B. S. Richards, M. Powalla, U. W. Paetzold, *Adv. Energy Mater.* **2019**, *9*, 1802995.

[22] H.-C. Liao, P. Guo, C.-P. Hsu, M. Lin, B. Wang, L. Zeng, W. Huang, C. M. M. Soe, W.-F. Su, M. J. Bedzyk, M. R. Wasielewski, A. Facchetti, R. P. H. Chang, M. G. Kanatzidis, T. J. Marks, *Adv. Energy Mater.* **2017**, *7*, 1601660.

[23] F. Di Giacomo, L. A. Castriotta, F. U. Kosasih, D. Di Girolamo, C. Ducati, A. Di Carlo, *Micromachines* **2020**, *11*, 1127.

[24] J. Y. Jeng, K. C. Chen, T. Y. Chiang, P. Y. Lin, T. D. Tsai, Y. C. Chang, T. F. Guo, P. Chen, T. C. Wen, Y. J. Hsu, *Adv. Mater.* **2014**, *26*, 4107.

[25] J. You, L. Meng, T.-B. Song, T.-F. Guo, Y. M. Yang, W.-H. Chang, Z. Hong, H. Chen, H. Zhou, Q. Chen, *Nat. Nanotechnol.* **2016**, *11*, 75.

[26] K.-C. Wang, J.-Y. Jeng, P.-S. Shen, Y.-C. Chang, E. W.-G. Diau, C.-H. Tsai, T.-Y. Chao, H.-C. Hsu, P.-Y. Lin, P. Chen, *Sci. Rep.* **2014**, *4*, 4756.
[27] B. G. Groeneveld, M. Najafi, B. Steensma, S. Adjokatse, H.-H. Fang, F. Jahani, L. Qiu, G. H. ten Brink, J. C. Hummelen, M. A. Loi, *Apl Materials* **2017**, *5*, 076103.
[28] Z. Zhu, Y. Bai, T. Zhang, Z. Liu, X. Long, Z. Wei, Z. Wang, L. Zhang, J. Wang, F. Yan, S. Yang, *Angew. Chem. Int. Ed. Engl.* **2014**, *53*, 12571.
[29] X. Yin, M. Que, Y. Xing, W. Que, *J. Mater. Chem. A* **2015**, *3*, 24495.
[30] W. Chen, Y. Wu, Y. Yue, J. Liu, W. Zhang, X. Yang, H. Chen, E. Bi, I. Ashraful, M. Grätzel, L. Han, *Science* **2015**, *350*, 944.
[31] F. Ye, H. Chen, F. Xie, W. Tang, M. Yin, J. He, E. Bi, Y. Wang, X. Yang, L. Han, *Energy Environ. Sci.* **2016**, *9*, 2295.
[32] E. Aydin, J. Troughton, M. De Bastiani, E. Ugur, M. Sajjad, A. Alzahrani, M. Neophytou, U. Schwingenschlögl, F. Laquai, D. Baran, S. De Wolf, *ACS Appl. Energy Mater.* **2018**, *1*, 6227.
[33] M. B. Islam, M. Yanagida, Y. Shirai, Y. Nabetani, K. Miyano, *ACS Omega* **2017**, *2*, 2291.
[34] S. Pang, C. Zhang, H. Dong, D. Chen, W. Zhu, H. Xi, J. Chang, Z. Lin, J. Zhang, Y. Hao, *ACS Appl. Energy Mater.* **2019**, *2*, 4700.
[35] T. Wang, D. Ding, X. Wang, R. Zeng, H. Liu, W. Shen, *ACS Omega* **2018**, *3*, 18434.
[36] I. J. Park, G. Kang, M. A. Park, J. S. Kim, S. W. Seo, D. H. Kim, K. Zhu, T. Park, J. Y. Kim, *ChemSusChem* **2017**, *10*, 2660.
[37] J. H. Park, J. Seo, S. Park, S. S. Shin, Y. C. Kim, N. J. Jeon, H.-W. Shin, T. K. Ahn, J. H. Noh, S. C. Yoon, C. S. Hwang, S. I. Seok, *Adv. Mater.* **2015**, *27*, 4013.
[38] S. Seo, I. J. Park, M. Kim, S. Lee, C. Bae, H. S. Jung, N.-G. Park, J. Y. Kim, H. Shin, *Nanoscale* **2016**, *8*, 11403.
[39] D. Koushik, M. Jošt, A. Dučinskas, C. Burgess, V. Zardetto, C. Weijtens, M. A. Verheijen, W. M. M. Kessels, S. Albrecht, M. Creatore, *J. Mater. Chem. C* **2019**, *7*, 12532.
[40] P. Ru, E. Bi, Y. Zhang, Y. Wang, W. Kong, Y. Sha, W. Tang, P. Zhang, Y. Wu, W. Chen, X. Yang, H. Chen, L. Han, *Adv. Energy Mater.* **2020**, *10*, 1903487.
[41] D. Di Girolamo, F. Di Giacomo, F. Matteocci, A. G. Marrani, D. Dini, A. Abate, *Chem. Sci.* **2020**, *11*, 7746.
[42] P. Chandrasekhar, Y.-H. Seo, Y.-J. Noh, S.-I. Na, *Appl. Surf. Sci.* **2019**, *481*, 588.
[43] S. S. Shin, S. J. Lee, S. I. Seok, *Adv. Funct. Mater.* **2019**, *29*, 1900455.
[44] B. Mustafa, J. Griffin, A. S. Alsulami, D. G. Lidzey, A. R. Buckley, *Appl. Phys. Lett.* **2014**, *104*, 29_1.
[45] J. H. Park, J. Seo, S. Park, S. S. Shin, Y. C. Kim, N. J. Jeon, H. W. Shin, T. K. Ahn, J. H. Noh, S. C. Yoon, *Adv. Mater.* **2015**, *27*, 4013.
[46] Z. Wang, P. K. Nayak, J. A. Caraveo-Frescas, H. N. Alshareef, *Adv. Mater.* **2016**, *28*, 3831.
[47] A. Corani, M.-H. Li, P.-S. Shen, P. Chen, T.-F. Guo, A. El Nahhas, K. Zheng, A. Yartsev, V. Sundström, C. S. Ponseca Jr, *J. Phys. Chem. Lett.* **2016**, *7*, 1096.
[48] Z. Yu, L. Sun, *Small Methods* **2018**, *2*, 1700280.
[49] X. Yin, Y. Guo, H. Xie, W. Que, L. B. Kong, *Sol. RRL* **2019**, *3*, 1900001.
[50] S. Sajid, A. M. Elseman, H. Huang, J. Ji, S. Dou, H. Jiang, X. Liu, D. Wei, P. Cui, M. Li, *Nano Energy* **2018**, *51*, 408.
[51] X. Liang, S. Bai, X. Wang, X. Dai, F. Gao, B. Sun, Z. Ning, Z. Ye, Y. Jin, *Chem. Soc. Rev.* **2017**, *46*, 1730.
[52] S. Liu, R. Liu, Y. Chen, S. Ho, J. H. Kim, F. So, *Chem. Mater.* **2014**, *26*, 4528.
[53] Y. Zhou, J. Hu, Y. Wu, R. Qing, C. Zhang, X. Xu, M. Jiang, *J. Photonics Energy* **2019**, *9*, 040901.
[54] R. Islam, G. Chen, P. Ramesh, J. Suh, N. Fuchigami, D. Lee, K. A. Littau, K. Weiner, R. T. Collins, K. C. Saraswat, *ACS Appl. Mater. Interfaces* **2017**, *9*, 17201.

[55] X. Yan, J. Zheng, L. Zheng, G. Lin, H. Lin, G. Chen, B. Du, F. Zhang, *Mater. Res. Bull.* **2018**, *103*, 150.
[56] J. R. Vig, *J. Vac. Sci. Technol., A* **1985**, *3*, 1027.
[57] Y. Sun, W. Chen, Y. Wu, Z. He, S. Zhang, S. Chen, *Nanoscale* **2019**, *11*, 1021.
[58] D. A. Hook, J. A. Olhausen, J. Krim, M. T. Dugger, *J. Microelectromech. Syst.* **2010**, *19*, 1292.
[59] J. Zhang, J. Wang, Y. Fu, B. Zhang, Z. Xie, *J. Mater. Chem. C* **2014**, *2*, 8295.
[60] F. Jiang, W. C. Choy, X. Li, D. Zhang, J. Cheng, *Adv. Mater.* **2015**, *27*, 2930.
[61] N. Pant, M. Yanagida, Y. Shirai, K. Miyano, *Appl. Phys. Express* **2020**, *13*, 025505.
[62] X. Zheng, Z. Song, Z. Chen, S. S. Bista, P. Gui, N. Shrestha, C. Chen, C. Li, X. Yin, R. A. Awni, *J. Mater. Chem. C* **2020**, *8*, 1972.
[63] J.-H. Tsai, I.-C. Cheng, C.-C. Hsu, J.-Z. Chen, *ACS omega* **2020**, *5*, 6082.
[64] Y. Nishihara, M. Chikamatsu, S. Kazaoui, T. Miyadera, Y. Yoshida, *Jpn. J. Appl. Phys.* **2018**, *57*, 04FS07.
[65] K. Wang, Y. Tian, H. Jiang, M. Chen, S. Xu, *Int. J. Photoenergy* **2019**, *2019*.
[66] J. H. Lee, Y. W. Noh, I. S. Jin, S. H. Park, J. W. Jung, *ACS Sustainable Chem. Eng.* **2019**, *7*, 15495.
[67] Q. Wang, C. C. Chueh, T. Zhao, J. Cheng, M. Eslamian, W. C. Choy, A. K. Jen, **2017**.
[68] J. Zhang, H. Luo, W. Xie, X. Lin, X. Hou, J. Zhou, S. Huang, W. Ou-Yang, Z. Sun, X. Chen, *Nanoscale* **2018**, *10*, 5617.
[69] H. Anizelli, T. W. David, P. Tyagi, E. Laureto, J. Kettle, *Sol. Energy* **2020**, *203*, 157.
[70] R. Kaneko, H. Kanda, K. Sugawa, J. Otsuki, A. Islam, M. K. Nazeeruddin, *Sol. RRL* **2019**, *3*, 1900172.
[71] J. Mangalam, T. Rath, S. Weber, B. Kunert, T. Dimopoulos, A. Fian, G. Trimmel, *J. Mater. Sci.: Mater. Electron.* **2019**, *30*, 9602.
[72] Z. Li, B. H. Jo, S. J. Hwang, T. H. Kim, S. Somasundaram, E. Kamaraj, J. Bang, T. K. Ahn, S. Park, H. J. Park, *Adv. Sci.* **2019**, *6*, 1802163.
[73] W. Chen, Y. Zhou, G. Chen, Y. Wu, B. Tu, F. Z. Liu, L. Huang, A. M. C. Ng, A. B. Djurišić, Z. He, *Adv. Energy Mater.* **2019**, *9*, 1803872.
[74] T. Wang, M. Xie, S. Abbasi, Z. Cheng, H. Liu, W. Shen, *J. Power Sources* **2020**, *448*, 227584.
[75] Y. Liu, J. Duan, J. Zhang, S. Huang, W. Ou-Yang, Q. Bao, Z. Sun, X. Chen, *ACS Appl. Mater. Interfaces* **2020**, *12*, 771.
[76] K. Choi, H. Choi, J. Min, T. Kim, D. Kim, S. Y. Son, G.-W. Kim, J. Choi, T. Park, *Sol. RRL* **2020**, *4*, 1900251.
[77] Y. Du, C. Xin, W. Huang, B. Shi, Y. Ding, C. Wei, Y. Zhao, Y. Li, X. Zhang, *ACS Sustainable Chem. Eng.* **2018**, *6*, 16806.
[78] I. J. Park, M. A. Park, D. H. Kim, G. D. Park, B. J. Kim, H. J. Son, M. J. Ko, D.-K. Lee, T. Park, H. Shin, N.-G. Park, H. S. Jung, J. Y. Kim, *J. Phys. Chem. C* **2015**, *119*, 27285.
[79] F. Wu, R. Pathak, C. Chen, Y. Tong, H. Xu, T. Zhang, R. Jian, X. Li, Q. Qiao, *Electrochim. Acta* **2020**, *354*, 136660.
[80] M. Li, X. Xu, Y. Xie, H.-W. Li, Y. Ma, Y. Cheng, S.-W. Tsang, *J. Mater. Chem. A* **2019**, *7*, 9578.
[81] B. Zhang, J. Su, X. Guo, L. Zhou, Z. Lin, L. Feng, J. Zhang, J. Chang, Y. Hao, *Adv. Sci.* **2020**, *7*, 1903044.
[82] Q. Niu, Y. Deng, D. Cui, H. Lv, X. Duan, Z. Li, Z. Liu, W. Zeng, R. Xia, W. Tan, Y. Min, *J. Mater. Sci.* **2019**, *54*, 14134.
[83] C. Chen, G. Yang, J. Ma, X. Zheng, Z. Chen, Q. Zhang, G. Fang, *J. Mater. Chem. C* **2017**, *5*, 10280.
[84] Y. Cheng, M. Li, X. Liu, S. H. Cheung, H. T. Chandran, H.-W. Li, X. Xu, Y.-M. Xie, S. K. So, H.-L. Yip, S.-W. Tsang, *Nano Energy* **2019**, *61*, 496.
[85] L. Soriano, I. Preda, A. Gutiérrez, S. Palacín, M. Abbate, A. Vollmer, *Phys. Rev. B* **2007**, *75*, 233417.

[86] Z. Zhu, Y. Bai, T. Zhang, Z. Liu, X. Long, Z. Wei, Z. Wang, L. Zhang, J. Wang, F. Yan, S. Yang, *Angew. Chem. Int. Ed.* **2014**, *53*, 12571.
[87] J. Cui, F. Meng, H. Zhang, K. Cao, H. Yuan, Y. Cheng, F. Huang, M. Wang, *ACS Appl. Mater. Interfaces* **2014**, *6*, 22862.
[88] W. Chen, Y. Wu, J. Liu, C. Qin, X. Yang, A. Islam, Y.-B. Cheng, L. Han, *Energy Environ. Sci.* **2015**, *8*, 629.
[89] C. Mrabet, M. B. Amor, A. Boukhachem, M. Amlouk, T. Manoubi, *Ceram. Int.* **2016**, *42*, 5963.
[90] G. Brunin, F. Ricci, V.-A. Ha, G.-M. Rignanese, G. Hautier, *npj Computational Materials* **2019**, *5*, 1.
[91] G. Guisbiers, S. Khanal, F. Ruiz-Zepeda, J. R. de la Puente, M. José-Yacaman, *Nanoscale* **2014**, *6*, 14630.
[92] K.-C. Wang, P.-S. Shen, M.-H. Li, S. Chen, M.-W. Lin, P. Chen, T.-F. Guo, *ACS Appl. Mater. Interfaces* **2014**, *6*, 11851.
[93] J. H. Kim, P.-W. Liang, S. T. Williams, N. Cho, C.-C. Chueh, M. S. Glaz, D. S. Ginger, A. K.-Y. Jen, *Adv. Mater.* **2015**, *27*, 695.
[94] W.-Y. Chen, J.-S. Jeng, K.-L. Huang, J.-S. Chen, *J. Vac. Sci. Technol.* **2013**, *31*, 021501.
[95] S. C. Chen, T. Y. Kuo, Y. C. Lin, H. C. Lin, *Thin Solid Films* **2011**, *519*, 4944.
[96] M. Feng, M. Wang, H. Zhou, W. Li, S. Wang, Z. Zang, S. Chen, *ACS Appl. Mater. Interfaces* **2020**, *12*, 50684.
[97] W. Chen, Y. Wu, J. Fan, A. B. Djurišić, F. Liu, H. W. Tam, A. Ng, C. Surya, W. K. Chan, D. Wang, Z.-B. He, *Adv. Energy Mater.* **2018**, *8*, 1703519.
[98] Q. He, K. Yao, X. Wang, X. Xia, S. Leng, F. Li, *ACS Appl. Mater. Interfaces* **2017**, *9*, 41887.
[99] R. Ishikawa, Y. Furuya, R. Araki, T. Nomoto, Y. Ogawa, A. Hosono, T. Okamoto, N. Tsuboi, *Jpn. J. Appl. Phys.* **2016**, *55*, 02BF04.
[100] J. Zheng, L. Hu, J. S. Yun, M. Zhang, C. F. J. Lau, J. Bing, X. Deng, Q. Ma, Y. Cho, W. Fu, C. Chen, M. A. Green, S. Huang, A. W. Y. Ho-Baillie, *ACS Appl. Energy Mater.* **2018**, *1*, 561.
[101] Y. Xie, K. Lu, J. Duan, Y. Jiang, L. Hu, T. Liu, Y. Zhou, B. Hu, *ACS Appl. Mater. Interfaces* **2018**, *10*, 14153.
[102] P.-H. Lee, B.-T. Li, C.-F. Lee, Z.-H. Huang, Y.-C. Huang, W.-F. Su, *Sol. Energy Mater. Sol. Cells* **2020**, *208*, 110352.
[103] X. Wan, Y. Jiang, Z. Qiu, H. Zhang, X. Zhu, I. Sikandar, X. Liu, X. Chen, B. Cao, *ACS Appl. Energy Mater.* **2018**, *1*, 3947.
[104] S. Wang, B. Zhang, D. Feng, Z. Lin, J. Zhang, Y. Hao, X. Fan, J. Chang, *J. Mater. Chem. C* **2019**, *7*, 9270.
[105] W. Chen, F.-Z. Liu, X.-Y. Feng, A. B. Djurišić, W. K. Chan, Z.-B. He, *Adv. Energy Mater.* **2017**, *7*, 1700722.
[106] X. Xia, Y. Jiang, Q. Wan, X. Wang, L. Wang, F. Li, *ACS Appl. Mater. Interfaces* **2018**, *10*, 44501.
[107] G. Li, Y. Jiang, S. Deng, A. Tam, P. Xu, M. Wong, H.-S. Kwok, *Adv. Sci.* **2017**, *4*, 1700463.
[108] W. Chen, Y. Wu, Y. Yue, J. Liu, W. Zhang, X. Yang, H. Chen, E. Bi, I. Ashraful, M. Grätzel, L. Han, *Science* **2015**, *350*, 944.
[109] S. Teo, Z. Guo, Z. Xu, C. Zhang, Y. Kamata, S. Hayase, T. Ma, *ChemSusChem* **2019**, *12*, 518.
[110] X. Chen, L. Xu, C. Chen, Y. Wu, W. Bi, Z. Song, X. Zhuang, S. Yang, S. Zhu, H. Song, *J. Power Sources* **2019**, *444*, 227267.
[111] Z. Hu, D. Chen, P. Yang, L. Yang, L. Qin, Y. Huang, X. Zhao, *Appl. Surf. Sci.* **2018**, *441*, 258.
[112] J. Zhang, W. Mao, X. Hou, J. Duan, J. Zhou, S. Huang, W. Ou-Yang, X. Zhang, Z. Sun, X. Chen, *Sol. Energy* **2018**, *174*, 1133.
[113] W. Nie, H. Tsai, J.-C. Blancon, F. Liu, C. C. Stoumpos, B. Traore, M. Kepenekian, O. Durand, C. Katan, S. Tretiak, J. Crochet, P. M. Ajayan, M. Kanatzidis, J. Even, A. D. Mohite, *Adv. Mater.* **2018**, *30*, 1703879.

[114] J. W. Jung, C.-C. Chueh, A. K.-Y. Jen, *Adv. Mater.* **2015**, *27*, 7874.
[115] P.-C. Chen, S.-H. Yang, *ACS Appl. Energy Mater.* **2019**, *2*, 6705.
[116] X. Yin, J. Han, Y. Zhou, Y. Gu, M. Tai, H. Nan, Y. Zhou, J. Li, H. Lin, *J. Mater. Chem. A* **2019**, *7*, 5666.
[117] K. Yao, F. Li, Q. He, X. Wang, Y. Jiang, H. Huang, A. K. Y. Jen, *Nano Energy* **2017**, *40*, 155.
[118] J. He, Y. Xiang, F. Zhang, J. Lian, R. Hu, P. Zeng, J. Song, J. Qu, *Nano Energy* **2018**, *45*, 471.
[119] Y. Zhang, S. Zhang, S. Wu, C. Chen, H. Zhu, Z. Xiong, W. Chen, R. Chen, S. Fang, W. Chen, *Adv. Mater. Interfaces* **2018**, *5*, 1800645.
[120] J. D. Hwang, T. H. Ho, *Mater. Sci. Semicond. Process.* **2017**, *71*, 396.

Table of Contents

Advances and Potentials of NiOx Surface Treatments for p-i-n Perovskite Solar Cells

Nidhi Tiwari,[a] Herlina Arianita Dewi[a], Enkhtur Erdenebileg[a], Ram Narayan Chauhan[b] Nripan Mathews, Subodh Mhaisalkar [a,c] and Annalisa Bruno[a]*

[a]Energy Research Institute @ NTU (ERI@N), Nanyang Technological University, Singapore 637553, Singapore
[b]Department of Physics, NIT Patna, India 800005
[c]School of Materials Science and Engineering, Nanyang Technological University, Singapore 637553, Singapore.

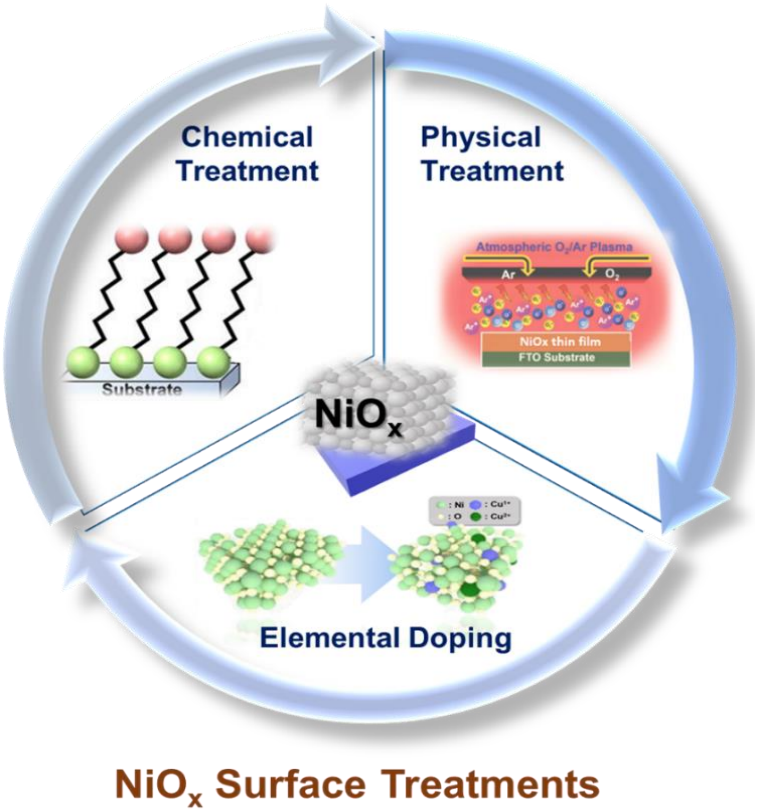

In this review, surface modifications based on *physical* (UV-ozone, oxygen, argon, and/or helium plasma), *chemical* (interlayer passivation), and *doping* treatments and their impacts on the structural and optoelectronic properties of the NiO_x are discussed. The effects of modified NiO_x films in p-i-n PSCs power conversion efficiency (PCE) are also examined together with the current challenges and future outlooks.